We are IntechOpen, the world's leading publisher of Open Access books Built by scientists, for scientists

6,900
Open access books available

185,000
International authors and editors

200M
Downloads

Our authors are among the

154
Countries delivered to

TOP 1%
most cited scientists

12.2%
Contributors from top 500 universities



WEB OF SCIENCE™

Selection of our books indexed in the Book Citation Index in Web of Science™ Core Collection (BKCI)

Interested in publishing with us?
Contact book.department@intechopen.com

Numbers displayed above are based on latest data collected.
For more information visit www.intechopen.com



Chapter

Deposition of Silver Nanoparticles on Indium Tin Oxide Substrates by Plasma-Assisted Hot-Filament Evaporation

Abtisam Hasan Hamood Al-Masoodi, Boon Tong Goh, Ahmed H.H. Al-Masoodi and Wan Haliza Binti Abd Majid

Abstract

Nanoparticles of noble metals have unique properties including large surface energies, surface plasmon excitation, quantum confinement effect, and high electron accumulation. Among these nanoparticles, silver (Ag) nanoparticles have strong responses in visible light region due to its high plasmon excitation. These unique properties depend on the size, shape, interparticle separation and surrounded medium of Ag nanoparticles. Indium tin oxide (ITO) is widely used as an electrode for flat panel devices in such as electronic, optoelectronic and sensing applications. Nowadays, Ag nanoparticles were deposited on ITO to improve their optical and electrical properties. Plasma-assisted hot-filament evaporation (PAHFE) technique produced high-density of crystalline Ag nanoparticles with controlling in the size and distribution on ITO surface. In this chapter, we will discuss about the PAHFE technique for the deposition of Ag nanoparticles on ITO and influences of the experimental parameters on the physical and optical properties, and electronic structure of the deposited Ag nanoparticles on ITO.

Keywords: silver nanoparticles, plasma-assisted hot-filament evaporation, properties, indium tin oxide, electronic structure

1. Introduction

Noble metallic nanoparticles, which are described as metals in the nanoscale with dimensions within size range from 1 to 100 nm, recently received significant attention in optoelectronic, biosensing and photocatalysts applications [1–4]. This is due to their unique properties compared to the bulk materials such as large surface energies, surface plasmon excitation, quantum confinement effect, and high electron accumulation. The bulk material has constant physical properties regardless of their size and shape, however, these properties of the nanoparticles are a function of their size, shape, distribution and surrounded medium. Among these nanoparticles, silver (Ag) nanoparticles have particularly strong responses in the visible light region due to its high plasmon excitation at threshold energy of around 3.9 eV (318 nm). A specific phenomenon of the nanoparticles is localized surface plasmon resonance (LSPR) which results from the collective oscillations of the free

electrons on the metallic nanoparticle surfaces. Thus, the LSPR of Ag nanoparticles can be tuned to any wavelength in the visible light region. This is a highly desirable characteristic enabling the usage of Ag nanoparticles in optoelectronic devices mainly in solar cell and light emitting diode devices [5, 6]. The LSPR wavelength position can be tuned by varying the size, shape, particle spacing and compositions of the nanoparticles as well as a surrounding environment such as an insulating surface or presence of a dielectric layer [7]. Oxide layer can be form around the nanoparticles and acts as dielectric substances leading to formation of metal–metal oxide core-shell nanoparticles. These core-shell nanoparticles have been reported to produce wide SPR bands compered to pure metallic nanoparticle [8, 9]. Thus, the wide range of the LSPR existing through the metal oxide layer could be better than increasing in the nanoparticles size that may significantly lead to reduction in light scattering. On the other hand, indium tin oxide (ITO) is a transparent conducting oxide that has high transparency in visible light regions, low sheet resistance, and high work function. Moreover, ITO is widely used as anode material for optoelectronic devices as a hole injection layer in the devices [10, 11]. Thus, deposition of Ag nanoparticles layer on ITO suggests a feasible approach to enhance the flexibility, luminescent efficiency, electrical conductivity, and adhesion to device layers.

Ag nanoparticles layer are widely synthesized using evaporation-condensation, electron beam irradiation, and radio frequency plasma-assisted thermal evaporation, which show a good surface adhesion with the dielectric surface [12–14]. However, these physical deposition methods generally involve complicated structures, surface treatments, and high reaction temperatures up to several thousand °C in a plasma jet and 400°C for thermal annealing purposes [13, 15, 16]. The high reaction temperatures usually lead to the destruction of the device layers during the deposition process [13, 15, 16]. This issue can be avoided using thermal evaporation by hot-filament, as it provides a rapid evaporation of metallic nanoparticles source in high purity and the most important is it involving low substrate temperatures (usually below 400°C) [17, 18]. Moreover, plasma-driven deposition controls the transportation and deposition of the evaporated metallic adatoms, which directly leads to better size and uniformity of the deposition [19]. Nevertheless, pre-plasma treatment on the substrate surface proved to be more effective in removing organic contaminations that impede the particle mobility on the deposited surface [20, 21]. Thus, plasma-assisted hot filament evaporation technique is expected to deposition of Ag nanoparticles layer in uniform size and distribution at low substrate temperatures.

2. Plasma-assisted hot-filament evaporation

Evaporation is a common method for deposition of thin film from their source materials in a vacuum as a physical vapor deposition (PVD) technique. The source materials are evaporated using evaporation source such as metal boat or coiled wire. Tungsten is a metal and has very high melting temperature about 3422°C. A tungsten wire can be coiled to form spiral shape for using as a hot-filament. This hot-filament is preferred to use for deposition very thin film compared to a tungsten boat. However, the deposition rate of the thin film on substrates using PVD technique is very low. Other common technique, chemical vapor deposition (CVD) is a technique for deposition nanostructured thin film on substrates with very high temperature using precursor gases [22]. Insertion of hot-filament in to the CVD technique helps to deposit nanocrystalline of nanostructured thin film at lower substrate temperature as hot-filament chemical vapor deposition (HFCVD) technique [18, 23–27]. The HFCVD process employs the heated filament to decompose

the precursor species and deposit nanostructured film on the substrate. On other hand, plasma can include electron, ions, free radicals, photons and neutrals that can generate reactive chemical species for enhancing the thin film deposition. The most recent technique was used is plasma-enhanced chemical vapor deposition (PECVD) [28–31]. However, PECVD requires a long time deposition and produces non-purity thin film with existence of toxic and explosive gases in plasma stream [32]. To avoid the existence of the toxic gases and contamination on the film, hydrogen plasma is used to remove the contaminations and provide purity thin film deposition without any toxic gases production. Therefore, hybrid of hot-filament with hydrogen plasma as plasma-assisted hot-filament evaporation (PAHFE) is a promise technique for deposition of purity metal nanoparticles layer on the substrate at low substrate temperature. Thus, the features of this technique are: (1) control of particle size, shape and interparticle separation, (2) enhancement of the nanoparticles crystallity, (3) stabilization in the physical and structure properties, (4) high deposition rate, (5) production of purity nanoparticles, (6) avoid particles aggregation, (7) low substrate temperature, and (8) fast deposition rate.

2.1 Structure of PAHFE

Figure 1(a) shows the real picture of the PAHFE system. The PAHFE consists to three main parts; reaction chamber, vacuum pumping system and supply units. The schematic diagram of the home-built of the reaction chamber is shown in **Figure 1(b)**. A radio frequency (RF) electrode was used as a plasma generation source. The tungsten wire with a diameter of 1 mm can be coiled to approximately 30 coils, generating coils with a diameter of 2 mm and length of 3 cm. This formed a tungsten coil filament as the hot-filament which the Ag source (Ag wire) was hanged on the filament coils for evaporation purpose. This hot-filament was placed below the RF electrode at a distance of 2 cm. Two copper electrodes were used to hang the tungsten wire, as shown in **Figure 1(b)**. Substrates which the nanoparticles deposited on were put on a substrate holder. The substrate holder was placed below the filament at a distance of 10 cm. After that, the substrates can be heated using a heater rod inserted into the substrate

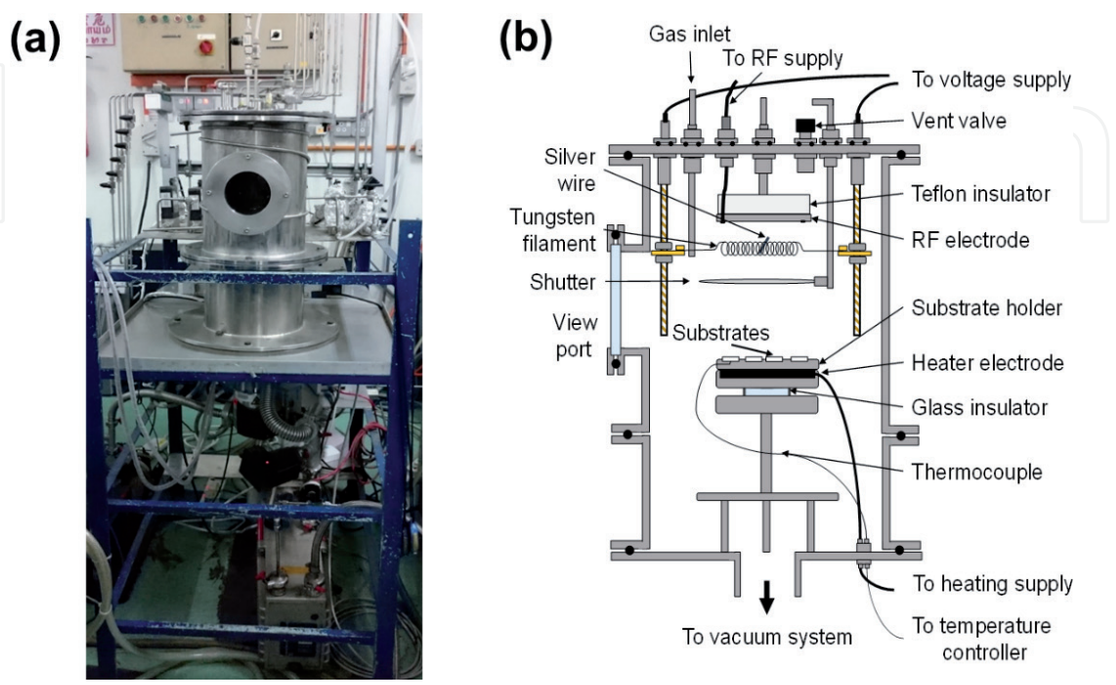


Figure 1.
(a) Real picture of PAHFE system. (b) Schematic diagram of the home-built PAHFE chamber [33].

holder for achieving a desired substrate temperature. A thermocouple was used to measure the substrate temperature and connected to a temperature controller. Finally, in order to control the evaporation time, a shutter was placed between the filament and substrate holder. There are four supply units for PAHFE technique. RF power supply of 13.56 MHz was connected to the RF electrode by a matching impedance for plasma generation in the reaction chamber. Filament heating power supply is used for heating the filament to a desired temperature in purpose of Ag wire evaporation. The two copper electrodes were connected to the filament heating power supply. Substrate heating power supply was connected to the heater rod to heat the substrate for achieving a particular substrate temperature. Finally, a hydrogen gas was supplied to the reaction chamber through ¼ inch SS tube and ball valve. The gas flow is precisely controlled by a mass flow-controller. Furthermore, the vacuum pumping system is used to evacuate the reaction chamber before and after deposition processes, and control the pressure as well.

2.2 Processes of PAHFE

Before placing the substrates inside the chamber, the substrates were put inside a beaker including Decon 90 diluted in deionized water to clean using ultrasound at 60°C for 60 minutes. Then, rinsing the substrates was sequentially done using deionized water, acetone and isopropyl alcohol. Finally, the clean substrates were dried using nitrogen gas. The Ag wire with a length of 2 mm and a diameter of 0.5 mm (Ag wire weight of 4.2 ± 0.2 mg and purity of 99.9%) was placed inside the coiled part of the filament. After placing the substrates inside the chamber, the chamber was evacuated to minimum or lowest pressure of around 5×10^{-3} Pa, using turbomolecular pump. Then, the substrates were heated to the desired substrate temperature. Before the nanoparticles deposition, plasma cleaning process was done on the substrate surface and Ag wire using hydrogen plasma. The parameters of the plasma cleaning process were put at 6 W, 100 sccm, 75 Pa, and 10 minutes for the RF power, hydrogen flow-rate, pressure, and time, respectively. In general, the hydrogen plasma process is utilized to remove any surface contaminants including native oxide on the substrates. After the plasma cleaning, the filament temperature was slowly increased to reach to 1600°C under hydrogen plasma ambient condition. The heated filament under plasma has sufficient thermal energy to completely evaporate the Ag wire which has a melting point of about 961°C. The deposition was started by opening the shutter subsequent to the plasma cleaning process as plasma deposition process. The RF power, hydrogen flow-rate, pressure, and time were fixed at 6 W, 50 sccm, 41 Pa, and 3 minutes, respectively. **Figure 2** shows the

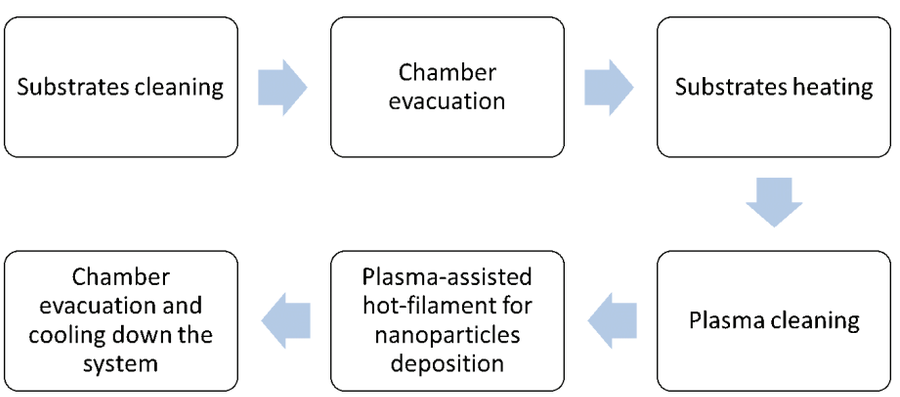


Figure 2.
Scheme of the PAHFE processes.

scheme of the PAHFE processes. The substrate temperature was varied between 25°C and 250°C at 25°C, 80°C, 140°C, 200°C, and 250°C.

3. Salient features of the deposited Ag nanoparticles on ITO substrate

The properties of Ag material in the nanoparticles form are different from the Ag bulk material due to consisting of the nanoparticles from down to few atoms. Thus, these few atoms may dominate of the nanoparticles properties. Also, distribution of the nanoparticles on a layer may strongly affect on their properties. This distribution of Ag nanoparticles on the layer depends on their size and interparticle separation. So, the nanoparticles could stand as a two-dimensional array to form Ag nanoparticles layer. Moreover, it is well-known LSPR characteristics of Ag nanoparticles that have unique optical properties in all visible region. This LSPR of Ag nanoparticles strongly depends on the physical properties of the Ag nanoparticles layer. Furthermore, PAHFE technique can control the properties of Ag nanoparticles layer by variation in growth parameters. Thus, the changing in these properties of the nanoparticles layer via the growth parameters is discussed, as mentioned below.

3.1 Morphological properties

The surface morphology including size, shape and distribution of Ag nanoparticles on the ITO/glass substrates, which can be obtained using field emission scanning electron microscopy (FESEM), varies with variation of the experimental parameters such as growth environment and substrate temperatures. FESEM images of the deposited Ag nanoparticles on ITO substrates at substrate temperature of 25°C without and with using plasma conditions during the deposition processes are presented in **Figure 3(a** and **b)**. These nanoparticles showed spherical shape in both conditions, and inconsistency size and interparticle separation distributions at no plasma condition compared with using plasma, as shown in

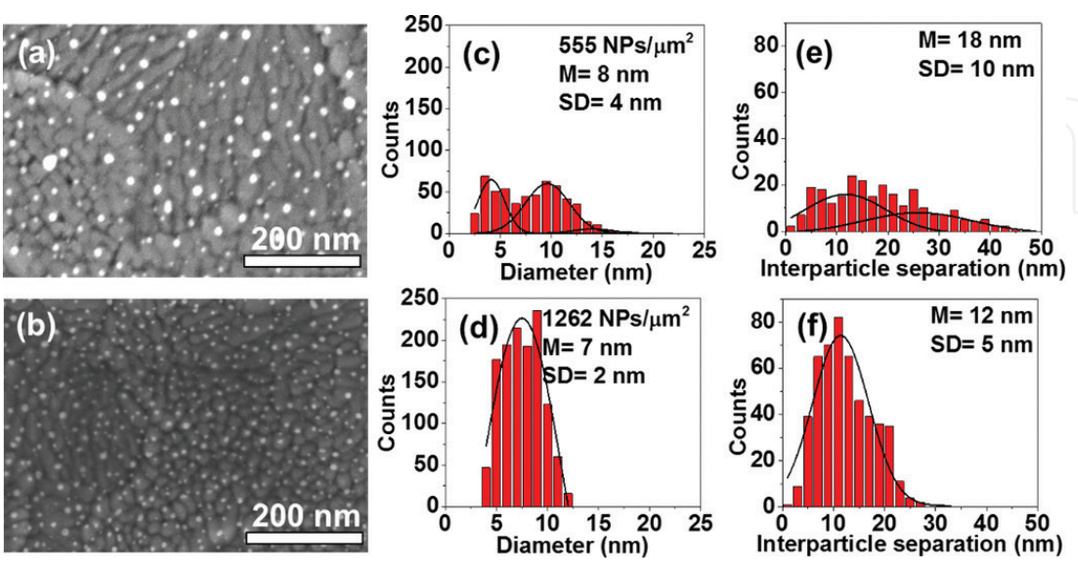


Figure 3.
(a and b) FESEM images, (c and d) histograms of diameter, and (e and f) histograms of interparticle separation of Ag nanoparticles deposited on ITO/glass substrates without and with using plasma at room temperature of the substrate temperature. The black solid lines in the histograms are the fitting Gaussian curves, and the nanoparticle density in NPs/μm² and the mean diameters or interparticle separations (M) with standard deviation (SD) values are inserted in each sub-figure.

Figure 3(c–f). Density of the nanoparticles at with plasma condition is about 1262 nanoparticles/μm^2 and showed higher than the density at without plasma condition (555 nanoparticles/μm^2). Thus, the combination of the hot-filament temperature and hydrogen ion plasma during the deposition assists to facilitate the growth of high density of Ag nanoparticles in uniform size and interparticle spacing. Moreover, the hot-filament temperature of 1600°C provided the evaporated Ag adatoms kinetic energy at low deposition pressure of 41 Pa. This thermal induced kinetic energy is sufficient to diffuse the Ag adatoms on the ITO surface for fast-forming of Ag nanoparticles at room temperature [34].

For variation in the substrate temperatures of 80, 140, 200 and 250°C with using plasma during the cleaning and deposition processes, the FESEM images of the deposited Ag nanoparticles on ITO substrates are presented in **Figure 4(a–d)**. In the substrate temperatures up to 140°C, Ag nanoparticles appeared to be also in spherical shape with high consistency in size and distribution. Also, the nanoparticles size increases with increasing in the temperature up to 140°C. This method is directly deposit the nanoparticles on surface in uniform size and interparticle separation without any additional process such as annealing process. This is in contrast

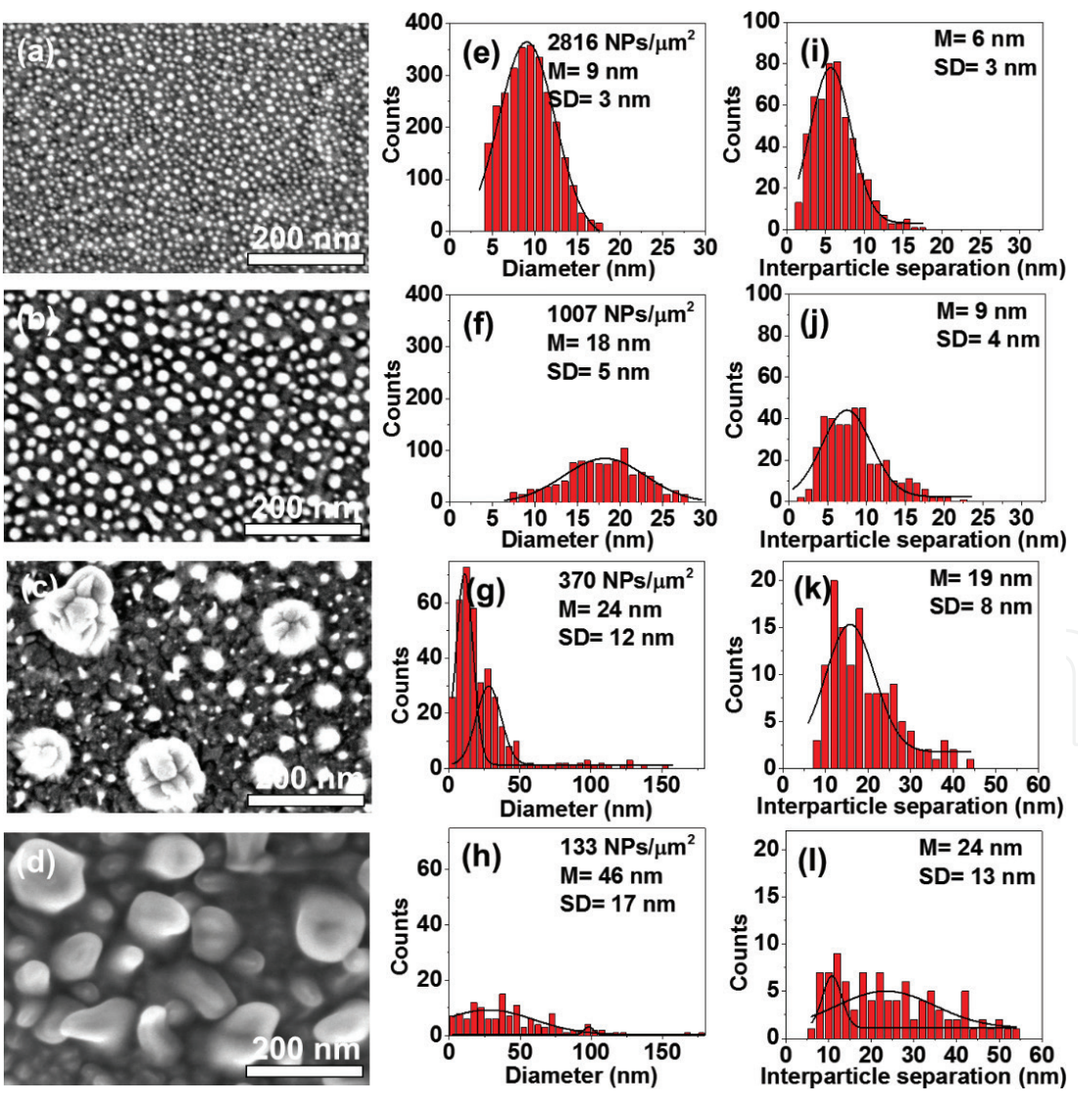


Figure 4.
(a–d) FESEM images, (e–h) histograms of diameter, (i–l) histograms of interparticle separation of Ag nanoparticles deposited on ITO/glass substrates using plasma with different substrate temperatures of 80°C, 140°C, 200°C, and 250°C, respectively. The black solid lines in the histograms are the fitting Gaussian curves, and the nanoparticle density in NPs/μm² and the mean diameters or interparticle separations (M) with standard deviation (SD) values are inserted in each sub-figure.

to the other nanoparticles formation methods obtained by other research studies which illustrated the nanoparticles formation of different sizes and interparticle separation as the temperature increased. Also, those methods required subsequent process of annealing temperature as an additional process that showed indirect deposition on the substrate surface [35–38]. Moreover, the substrate temperature provides sufficient surface mobility to the deposited Ag nanoparticles for diffusion into their growth sites and coalescing to form larger particles [39]. In addition, the ionized hydrogen radicals in the plasma deposition can transfer their kinetic energies to the ITO surface leading to increase the surface diffusion of Ag adatoms that enhances the uniform distribution of the deposited Ag nanoparticles on the ITO surface. Density of the deposited Ag nanoparticles decreases with increase in the substrate temperature, with the highest density of Ag nanoparticles obtained at 80°C compared to the room temperature (**Figures 3(d)** and **4(e)**). This indicates that the substrate temperature of ITO/glass provides sufficient surface mobility for the Ag adatoms to form Ag nanoparticles with the highest density at 80°C. Moreover, the substrate temperature at 200°C and 250°C, the size of the nanoparticles increased in a non-uniformity and an inconsistent interparticle distribution, as seen in **Figure 4(c** and **d)**. The hydrogen plasma can etch out oxygen bonded to the ITO surface leading to formation of SnO and In_2O_3 particles at higher substrate temperatures more than the melting temperatures of In (156.6°C) and Sn (231.9°C). Then, the oxygen adatoms diffused to the Ag nanoparticles resulting in formation of Ag oxide layer [40]. These oxide layer and SnO and In_2O_3 particles appeared the nanoparticles in non-uniformity in the size and shape (**Figure 4(c** and **d)**). The area filling fraction is represented by the ratio of the nanoparticles area to the substrate area [41]. The calculated area filling fractions for the nanoparticles were 20.79, 26.96, 32.35, and 34.65% at substrate temperatures of 80°C, 140°C, 200°C, and 250°C, respectively. The increase in the area filling fraction of Ag nanoparticles with decreasing in the density as the substrate temperature increases on ITO/glass substrate is due to the increase in the size with decrease in interparticle separation, as shown in **Figure 4(e–l)**. Therefore, the physical properties of Ag nanoparticles on ITO substrates can be simply controlled by fine-tuning in the substrate temperature to below 200°C with using plasma during the growth processes.

3.2 Structural properties

The deposition of Ag nanoparticles on the oxide substrate under hydrogen plasma may affect on the composition of the nanoparticles. The nanoparticles structure can be recorded via X-ray diffraction (XRD) patterns. **Figure 5** shows the XRD patterns of the Ag nanoparticles deposited on ITO/glass substrates at different substrate temperatures. ITO diffraction peaks are obviously presented in prepared sample at 25°C with diffraction peaks shown in **Figure 5**, according to JCPDS card no. 01-089-4596. These diffraction peaks of ITO significantly decrease with increasing in the temperature due to the plasma etching on the ITO surface. A small noticeable diffraction peak at 32.8°, which corresponds to the Ag_2O crystalline plane of (111) according to JCPDS card no. 41-1104, appeared at all samples and increases with increasing in the temperature. An additional diffraction peak of Ag_2O at 68.8° for the crystalline plane of (222) can be observed at temperatures above 200°C. Moreover, AgO diffraction peaks are also observed in the prepared samples at all substrate temperatures above 80°C. These diffraction peaks of AgO located at 39.4, 56.88, and 67.3° correspond to the crystalline planes of (−202), (−113), and (−313), according to JCPDS card no. 022-0472. Moreover, very small diffraction peaks of metallic Ag appeared at 38.1 and 44.3° indicated to crystallographic planes of (111) and (200), respectively. The emergence of AgO and Ag_2O peaks is due to the

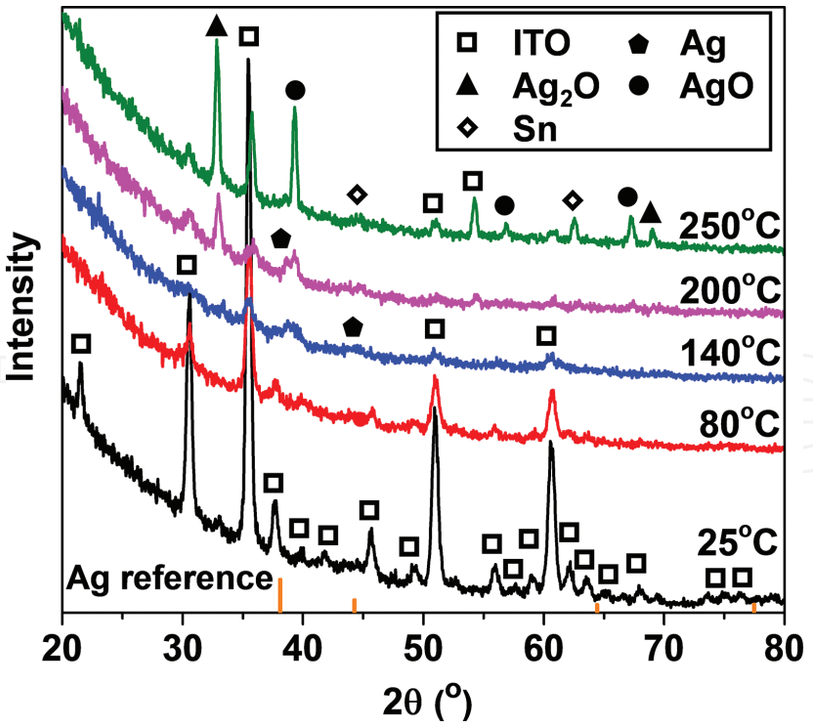


Figure 5.
XRD patterns of Ag nanoparticles deposited on ITO/glass substrates at different substrate temperatures. The reference of bulk Ag is provided in the figure [33].

ejection of oxygen adatoms from the ITO surface by hydrogen etching in ambient plasma at higher substrate temperature leading to oxidation of the Ag nanoparticle surface. Thus, the Ag oxide is formed as a shell and the metallic Ag is as a core of the nanoparticles. The crystallite sizes of Ag_2O are 4.04, 7.94, 13.19, 17.92 and 21.13 nm for different substrate temperatures of 25, 80, 140, 200 and 250°C, respectively, while the crystallite sizes of AgO appeared at 140, 200 and 250°C to be 7.29, 15.29 and 22.45 nm, respectively. The increasing in the crystallite sizes of the Ag oxides is due to the increasing in the diffusion of oxygen adatoms into Ag nanoparticles during the deposition processes. In addition, small diffraction peaks at 44.9 and 62.5° were obviously appeared at 250°C. These diffraction peaks belong to the crystalline planes of metallic Sn (according to JCPDS card no.00-004-0673 for crystalline plane of (211) and (112), respectively). These metallic Sn diffraction peaks indicate to the formation of Sn particles due to the hydrogen plasma etching effect at higher substrate temperature.

The chemical materials of the deposited Ag nanoparticles on ITO surface can be obtained by a wide scan of X-ray photoemission spectroscopy (XPS), as shown in **Figure 6(a)**. The wide scan of XPS of the deposited Ag nanoparticles on ITO substrate exhibited the presence of ITO, Ag and carbon materials. The existence of the carbon material is attributed to adventitious carbon which is normally present in all air-exposed materials. Thus, PAHFE technique is a suggested method to deposit pure Ag nanoparticles without any additional materials which usually exist during the synthesis process. The narrow-scan of Ag materials for different substrate temperatures is presented in **Figure 6(b)**. The highest XPS peak was at 80°C due to the highest density of the nanoparticles. Then, the XPS peaks decrease with the substrate temperature more than 80°C and disappeared at 200 and 250°C. This means that Ag nanoparticles diffuse away from the ITO surface at higher temperatures due to incorporation of SnO and In_2O_3 particles as shell layers onto the Ag nanoparticles. Li et al. have reported decreasing in the Ag content at heat-treatment temperature above 300°C due to the diffusion of Ag nanoparticles away

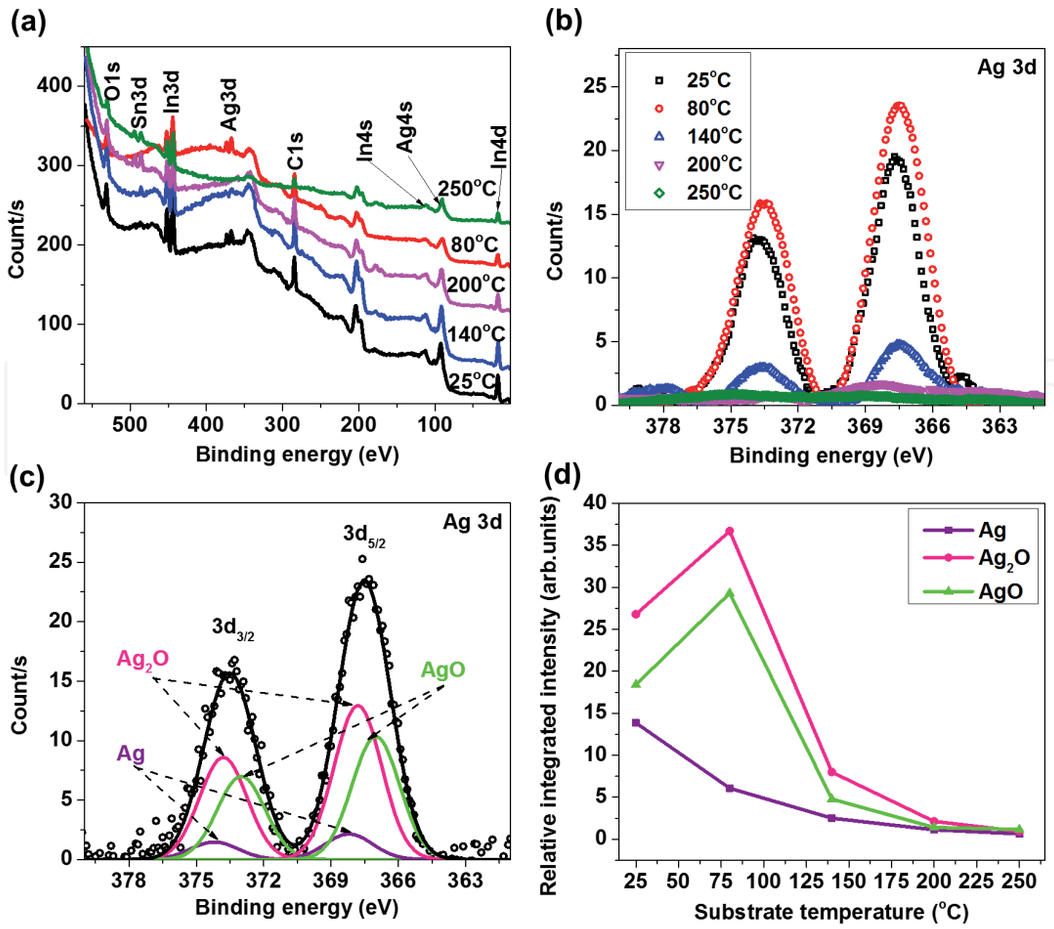


Figure 6.
(a) Wide-scan and (b) Ag 3d narrow-scan of the XPS spectra for Ag nanoparticles deposited on ITO/glass substrates at different substrate temperatures. (c) Typical deconvoluted components to their binding energies of Ag 3d narrow-scan, and (d) variations of the respective deconvoluted components against the substrate temperature.

from surface [42]. In **Figure 6(c)**, the XPS peak of Ag 3d was deconvoluted into three components located at 368.2, 367.8, and 367 eV (Ag $3d_{5/2}$), corresponding to the Ag's metallic state and the two oxidation states of AgO and Ag_2O [43–45]. These Ag oxidation states caused by the formation of AgO and Ag_2O attributed to the diffusion of surface oxide from the ITO substrate, forming a metallic oxide layer on the nanoparticles. The variations of relative integrated intensity for the Ag deconvoluted components are plotted against substrate temperatures in **Figure 6(d)**. The oxidation of Ag nanoparticles is maximal at the substrate temperature of 80°C, forming AgO and Ag_2O shell layers on the nanoparticles and shows decreasing with increasing in the substrate temperature due to the covering by SnO and In_2O_3 materials on the Ag nanoparticles as shell layers at higher temperatures.

3.3 Optical properties

Optical properties of Ag nanoparticles layer are dependent on their sizes and interparticle separations which are dependent on the experimental parameters. The optical absorbance and transmittance can be examined by UV–VIS–NIR spectrophotometer. **Figure 7** showed the optical absorbance and transmittance of the deposited Ag nanoparticles on ITO substrates with using plasma and no plasma conditions at room temperature of the substrate temperature. The absorbance spectra showed one peak for deposited Ag nanoparticles with plasma and three peaks for no plasma condition. This means the deposited Ag nanoparticles at plasma condition appeared as isolated nanoparticles while at no plasma condition

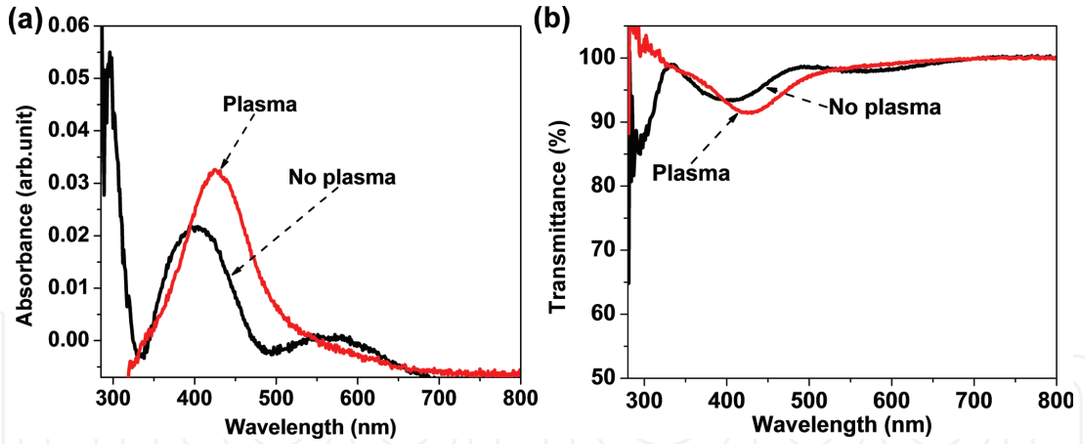


Figure 7.
(a) Absorbance and (b) transmittance spectra of Ag nanoparticles deposited on ITO with plasma and no plasma conditions at room temperature of the substrate temperature.

exhibited a coupled nanoparticles for the two shorter wavelength with appearance larger particles for the third wavelength. The isolated Ag nanoparticles have larger interparticle separations than its diameter while the coupled nanoparticles have smaller interparticle separation than its diameter [46]. The LSPR peak of these isolated Ag nanoparticles deposited with plasma condition showed wide spectrum and centred around 426 nm. However, the nanoparticles size is slightly less than 10 nm that leads to the sharp LSPR peak to be appeared around 400 nm [46]. These shift and wideness are due the formation of Ag oxide as a shell around Ag nanoparticles [8, 47]. Moreover, the intensity of spectrum for with plasma condition appeared higher than no plasma condition that means the deposition higher nanoparticles density at with plasma condition.

For the different substrate temperature with using plasma parameters, the optical absorbance and transmittance spectra of the deposited Ag nanoparticles on ITO substrates are depicted in **Figure 8(a** and **b)**. The SPR peak located at 320 nm remains constant with the change in substrate temperature owing to the absorption coming from the ITO/glass substrate [48]. The SPR peak at 140°C showed slight blue shift with higher intensity compared to at 80°C of the substrate temperature. This slight blue shift is due to a reduction in the interparticle separation to diameter ratio with increasing in the diameter, while the higher intensity belongs to higher area filling fractions for Ag nanoparticles [49]. The absorbance spectra at higher substrate temperature appeared interference fringes in the visible region due to coherent multiple reflections on the ITO surface. The appearance of these reflections comes from the ITO surface decomposition via hydrogen plasma with hot-filament at above 80°C leading to increase in the interference and absorption peaks of ITO with temperature. The transmission spectra show high transmittance at 80 and 140°C and very low at substrate temperature up to 200°C and 250°C. This low transmittance belong to increase in the nanoparticles size leading to larger scattering of light. The interference of ITO decomposition and absorption peaks of Ag nanoparticles were fitted by Gaussian fitting components as demonstrated in **Figure 8(c)**. The appearance of two significant SPR peaks is due to the assembly of Ag nanoparticles as coupled nanoparticles.

The SPR peaks of the deposited Ag nanoparticles on ITO surface in different plasma deposition and Ag wire sizes are shown in **Figure 9(a** and **b)**, respectively. The SPR peak increases with red shift for increasing in the plasma deposition of 12, 18 and 24 W at room temperature of the substrate temperature, as presented in **Figure 9(a)**. The high intensity refers to higher area filling fractions for the

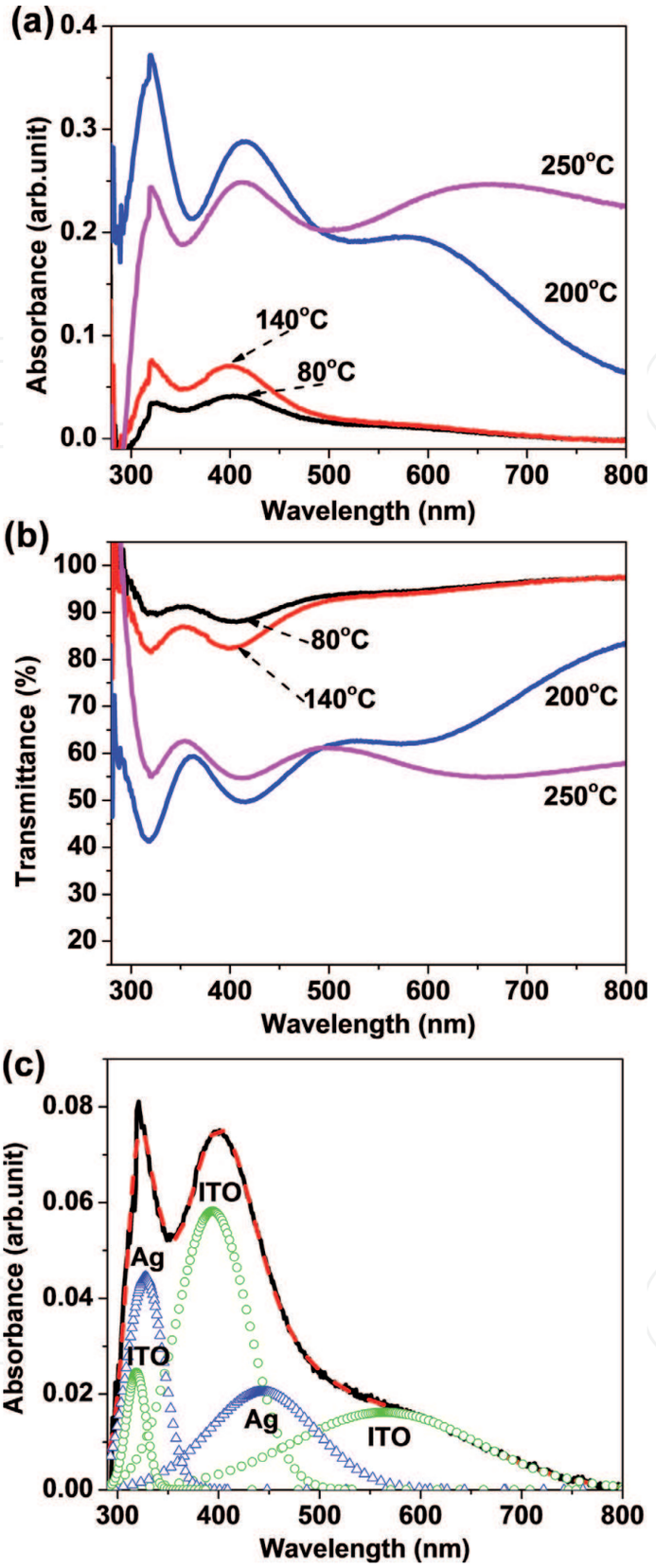


Figure 8.
(a) Absorbance and (b) transmittance spectra of Ag nanoparticles deposited on ITO with using plasma at different substrate temperatures. (c) Gaussian deconvolution of absorbance spectrum for Ag nanoparticles deposited on ITO/glass substrates at 140°C [33].

deposited Ag nanoparticles and the red shift belongs to increases in the nanoparticles size for isolated nanoparticles at 12 and 18 W of plasma deposition. There is a small peak appeared in shorter wavelength at 24 W that means the appearance of

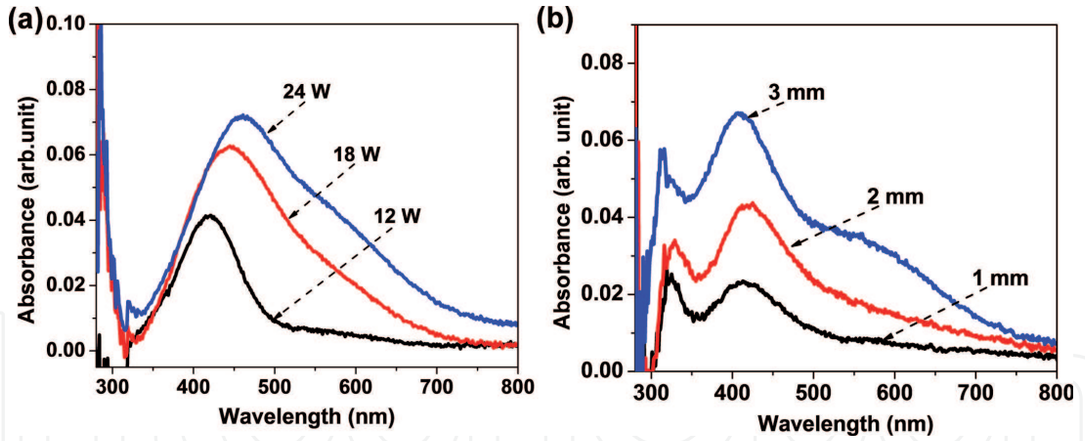


Figure 9.
Absorbance spectra of Ag nanoparticles deposited on ITO surface at (a) different plasma deposition at 25°C, and (b) different Ag wire size at 100°C.

the coupled nanoparticles at higher plasma deposition. For different Ag wire sizes shown in **Figure 9(b)**, the absorbance peaks increase in the intensity with increasing in the Ag wire sizes that belong to increasing in the area filling fractions for the deposited Ag nanoparticles by increasing in the nanoparticles size. The shorter peak showed slight red shift at 2 mm and blue shift at 3 mm of Ag wire size while the middle peak exhibited slight blue shift with appearance of a third peak at 3 mm of Ag wire size. These peaks resulted from the overlapping of the SPR of Ag nanoparticles with the ITO interference due to the substrate temperature of 100°C, and the shifts refer to gradually decreasing in the interparticle separation to diameter ratios at 2 mm and 3 mm, respectively.

3.4 Electronic structure

The optical band gap for ITO with Ag nanoparticles prepared at 25, 80, 140, 200, 250°C of substrate temperatures are about 4.131, 4.097, 4.076, 4.098 and 4.134 eV, respectively [33]. The decreasing of the optical energy gap of the ITO with Ag nanoparticles compared to the determined band gap of the ITO around 4.153 eV is due to the small band gap of Ag_2O and AgO about 1.46 and 1.7 eV, respectively [50, 51]. The small change in the optical band gap is due to the small area filling fraction of the nanoparticles on ITO surface. Moreover, the work function for ITO with Ag nanoparticles prepared at 25, 80, 140, 200, 250°C of substrate temperatures are about 4.18, 3.97, 4.19, 4.29 and 3.26 eV, respectively. These work functions showed slightly lower than the pure ITO work function (4.72 eV) due to the work function of Ag polycrystalline of 4.26 eV [52]. Moreover, the slight reduction in the work function at 80°C is due to the increasing in the crystallite size of Ag_2O, and the slight increment in the work functions at 140 and 200°C are due to the formation of AgO [53]. Furthermore, a reduction in work function to 3.26 eV was noticed in the ITO with Ag nanoparticles prepared at substrate temperature of 250°C. This reduction is due to the decomposition of ITO at higher temperature resulting in the formation of ITO nanoparticles, which have been reported its work function lower than work function of the bulk material (~3.8 eV) [54]. In addition, it is known that the work function is the energy difference between the Fermi level and the vacuum level, and increasing in the work function leads to improvement in electronic conductivity [55]. However, the Ag oxide leads to loss of electrons compared to the metallic Ag due to the reduction in the Fermi level edge [53]. **Figure 10** shows the energy levels diagram of pure ITO and ITO with Ag nanoparticles. The increasing in the energy difference of ITO with Ag nanoparticles compared to pure ITO has

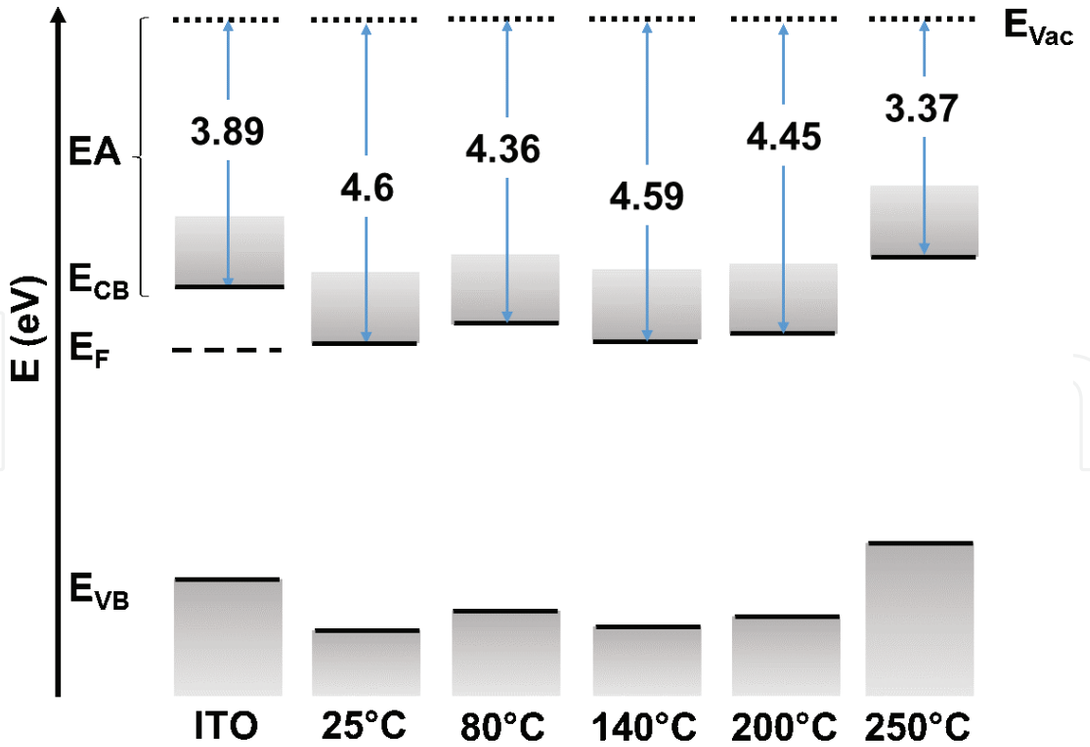


Figure 10.
Energy level diagrams of Ag nanoparticles deposited on ITO/glass substrates at different substrate temperatures and blank ITO substrate, respectively. The valence band energy E_{VB}, Fermi energy E_F, conduction band energy E_{CB}, electron affinity EA, and vacuum level energy E_{Vac} are indicated in the figure [33].

been reported to be null due to an increasing in quantity of free electrons in the Fermi level [33].

3.5 Electrical properties

The distribution of small size of Ag nanoparticles on a layer does not conduct electricity efficiently. However, deposition of these nanoparticles on conducting layer (ITO) may affect on the surface conductivity of the conducting layer. The sheet resistances of ITO surface with Ag nanoparticles prepared with using plasma at different substrate temperatures of 25, 80, 140, 200, 250°C are about 7.75, 7.45, 8, 8.87 and 16.91 Ohm/square, respectively [33]. At the substrate temperature below 200°C, there is no significant effect in the sheet resistances of ITO with Ag nanoparticles and pure ITO (7.68 Ohm/square). However, the sheet resistance of ITO with Ag nanoparticles showed increasing at substrate temperature of 250°C. This increment in the sheet resistance have been reported for ITO particles with thickness of approximately 20 μm to be about 15 ± 5 Ohm/square [56]. Moreover, the resistance sensitivities of AgO and Ag_2O have been reported to be about 50 and 12.5 Ohm.m, respectively [57–59]. Thus, the increasing in the Ag oxidation and the formation of In_2O_3 and SnO particles lead to change in sheet resistance for ITO with Ag nanoparticles at 250°C resulting in increasing in the contact resistance between the Ag nanoparticles and ITO.

4. Growth mechanism

The formation of Ag nanoparticles at different substrate temperatures using PAHFE technique was sequentially clarified in two processes, plasma cleaning and plasma deposition. For the plasma cleaning, a high energetic hydrogen ions as a

hydrogen plasma was run for 10 minutes. This hydrogen plasma acts to remove the oxide contaminations from the ITO and Ag wires surfaces as well as activate the substrate surfaces [60, 61]. After the plasma cleaning, high density of remaining surface bonded oxygen was produced on the ITO top and sup-layers and increases with rising in the substrate temperature. Increasing in surface bonded oxygen on the ITO leads to form In_2O_3 and SnO columnar grains at higher temperatures. For plasma deposition, the hot filament was run with the hydrogen plasma for evaporation Ag wire under plasma environment. The thermal energetic of the evaporated Ag adatoms were reached to the ITO surface to form Ag nanoparticles with oxide shell layers of Ag_2O and AgO due to the high-density bonded oxygen surfaces. Moreover, the Ag adatoms have a limited surface mobility on high density bonded oxygen surfaces. Thus, the low substrate temperatures lead to the nanoparticles formation with oxide shell layers due to low bonding energies of Ag-Ag and Ag-O of more than 163 and 213 eV, respectively [62].

The decomposition of ITO surface into SnO and In_2O_3 particles can be observed at substrate temperature more than 200°C due to the low melting points of In and Sn which are 156.6 and 231.9°C, respectively. The hydrogen plasma facilitates the surface decomposition of ITO leading to increase of oxygen adatoms in the nucleation sites [33]. Moreover, increasing in the substrate temperatures leads to increase in surface diffusion of the surface oxygen adatoms into the decomposed sites of ITO resulting in formation of large particles of In_2O_3 and SnO. Furthermore, the bonding energy of SnO (528 eV) is more stable than In_2O_3 (360 eV) at higher substrate temperature of 250°C. Thus, the oxygen surface diffusion with decomposition of ITO enhances the formation of SnO nanoparticles leading to reducing in the AgO, Ag_2O, and In_2O_3 nanoparticles on the surface at higher substrate temperatures.

5. Conclusion

Ag nanoparticles layer were deposited on ITO substrates via PAHFE technique at low substrate temperatures less than 200°C. This technique is simple and fast deposition which required approximately 3 minutes of the deposition time and showed directly formation of the nanoparticles layer from the pure Ag wire source. The size and interparticle separation of Ag nanoparticles can be controlled by variation in the experimental parameters. The morphological, structural, optical, and electrical properties of the Ag nanoparticles produced were also studied. Using plasma during the deposition leads to formation of uniform size and distribution of Ag nanoparticles. The nanoparticles growth rate was induced by increasing in the substrate temperature up to 140°C leading to increasing in the nanoparticles size and interparticle separation. The oxygen adatoms can diffuse to the nanoparticles to form Ag oxide shell which was enhanced by the plasma ambient and substrate temperature. Moreover, the SPR of the nanoparticles was strongly dependent on the diameter and interparticle separation of the nanoparticles. In addition, the high population of the Ag nanoparticles at 80°C improved the surface conductivity for the ITO with Ag nanoparticles to be at 7.45 Ohm/square and decreased the work function to 3.97 eV. However, the formation of SnO and In_2O_3 particles at the substrate temperature of 250°C increased the sheet resistance to 16.91 Ohm/square and more decreasing in the work function to 3.26 eV. Furthermore, the variation in the experimental parameters using PAHFE technique was observed to tune the optical and electrical properties of ITO with Ag core and Ag oxide shell nanoparticles resulting in changes in the functionality of Ag nanoparticle-coated transparent conductive oxide thin films to be useful in the applications of the optoelectronic devices.

Acknowledgements

This work was supported by the University of Malaya UMRG Programme - Frontier Science (RP038C-17AFR) and the University of Malaya Research Partnership Grant (RK006-2019). We would also like to thank the SLRI BL3.2a beamline staffs that help us in measuring XPS and UPS.

IntechOpen

Author details

Abtisam Hasan Hamood Al-Masoodi[1*], Boon Tong Goh[1], Ahmed H.H. Al-Masoodi[2] and Wan Haliza Binti Abd Majid[1]

1 Low Dimensional Materials Research Center, Department of Physics, Faculty of Science, University of Malaya, 50603 Kuala Lumpur, Malaysia

2 Department of Electronic and Telecommunication Engineering, College of Engineering, The American University of Kurdistan, 42001 Duhok, Kurdistan Region of Iraq

*Address all correspondence to: abtalmasoodi@gmail.com

IntechOpen

© 2020 The Author(s). Licensee IntechOpen. This chapter is distributed under the terms of the Creative Commons Attribution License (http://creativecommons.org/licenses/by/3.0), which permits unrestricted use, distribution, and reproduction in any medium, provided the original work is properly cited. CC BY

References

[1] Ko S-J, Choi H, Lee W, Kim T, Lee BR, Jung J-W, et al. Highly efficient plasmonic organic optoelectronic devices based on a conducting polymer electrode incorporated with silver nanoparticles. Energy & Environmental Science. 2013;**6**:1949-1955

[2] Liang Z, Sun J, Jiang Y, Jiang L, Chen X. Plasmonic enhanced optoelectronic devices. Plasmonics. 2014;**9**:859-866

[3] Naghib SM. Fabrication of nafion/silver nanoparticles/reduced graphene nanosheets/glucose oxidase nanobiocomposite for electrochemical glucose biosensing. Anal. Bioanal. Electrochem. 2016;**8**:453-465

[4] Awazu K, Fujimaki M, Rockstuhl C, Tominaga J, Murakami H, Ohki Y, et al. A plasmonic photocatalyst consisting of silver nanoparticles embedded in titanium dioxide. Journal of the American Chemical Society. 2008;**130**:1676-1680

[5] Fukuura T. Plasmons excited in a large dense silver nanoparticle layer enhance the luminescence intensity of organic light emitting diodes. Applied Surface Science. 2015;**346**:451-457

[6] Kalfagiannis N, Karagiannidis P, Pitsalidis C, Panagiotopoulos N, Gravalidis C, Kassavetis S, et al. Plasmonic silver nanoparticles for improved organic solar cells. Solar Energy Materials and Solar Cells. 2012;**104**:165-174

[7] Noguez C. Surface plasmons on metal nanoparticles: The influence of shape and physical environment. The Journal of Physical Chemistry C. 2007;**111**:3806-3819

[8] Schinca D, Scaffardi L, Videla F, Torchia G, Moreno P, Roso L. Silver–silver oxide core–shell nanoparticles by femtosecond laser ablation: Core and shell sizing by extinction spectroscopy. Journal of Physics D: Applied Physics. 2009;**42**:215102

[9] Lok C-N, Ho C-M, Chen R, He Q-Y, Yu W-Y, Sun H, et al. Silver nanoparticles: Partial oxidation and antibacterial activities. JBIC Journal of Biological Inorganic Chemistry. 2007;**12**:527-534

[10] Lee J, Jung B-J, Lee J-I, Chu HY, Do L-M, Shim H-K. Modification of an ITO anode with a hole-transporting SAM for improved OLED device characteristics. Journal of Materials Chemistry. 2002;**12**:3494-3498

[11] Kuwabara T, Nakayama T, Uozumi K, Yamaguchi T, Takahashi K. Highly durable inverted-type organic solar cell using amorphous titanium oxide as electron collection electrode inserted between ITO and organic layer. Solar Energy Materials and Solar Cells. 2008;**92**:1476-1482

[12] Kimoto K, Kamiya Y, Nonoyama M, Uyeda R. An electron microscope study on fine metal particles prepared by evaporation in argon gas at low pressure. Japanese Journal of Applied Physics. 1963;**2**:702

[13] Park ST, Kim T-H, Park D-W. Influence of injected silver content on synthesis of silver coated nickel particles by DC thermal plasma. Applied Surface Science. 2016;**374**:257-264

[14] Bogle K, Dhole S, Bhoraskar V. Silver nanoparticles: Synthesis and size control by electron irradiation. Nanotechnology. 2006;**17**:3204

[15] Suh J, Han B, Kim DS, Choi M. A method for enhanced charging of nanoparticles via condensation

magnification. Journal of Aerosol Science. 2005;**36**:1183-1193

[16] Azizian-Kalandaragh Y, Nouhi S, Amiri M. Effect of post-annealing treatment on the wetting, optical and structural properties of Ag/indium tin oxide thin films prepared by electron beam evaporation technique. Materials Express. 2015;**5**:137-145

[17] Nazarudin NFFB, Azizan SNAB, Rahman SA, Goh BT. Growth and structural property studies on NiSi/SiC core-shell nanowires by hot-wire chemical vapor deposition. Thin Solid Films. 2014;**570**:243-248

[18] Al-Masoodi AHH, Hamzan NB, Al-Masoodi AHH, Rahman SA, Goh BT. Influences of hydrogen dilution on the growth of Si-based core–shell nanowires by HWCVD, and their structure and optical properties. Applied Physics A. 2016;**122**:239

[19] Teo KB, Hash DB, Lacerda RG, Rupesinghe NL, Bell MS, Dalal SH, et al. The significance of plasma heating in carbon nanotube and nanofiber growth. Nano Letters. 2004;**4**:921-926

[20] Thomas R, Mantini M, Rudder R, Malta D, Hattangady S, Markunas R. Carbon and oxygen removal from silicon (100) surfaces by remote plasma cleaning techniques. Journal of Vacuum Science & Technology A: Vacuum, Surfaces, and Films. 1992;**10**:817-822

[21] Baker M. Plasma cleaning and the removal of carbon from metal surfaces. Thin Solid Films. 1980;**69**:359-368

[22] Mathur S, Sivakov V, Shen H, Barth S, Cavelius C, Nilsson A, et al. Nanostructured films of iron, tin and titanium oxides by chemical vapor deposition. Thin Solid Films. 2006;**502**:88-93

[23] Nazarudin NFFB, Noor NJBM, Rahman SA, Goh BT. Photoluminescence and structural properties of Si/SiC core–shell nanowires growth by HWCVD. Journal of Luminescence. 2015;**157**:149-157

[24] binti Hamzan N, bin Ramly MM, Huang NM, Rahman SA, Goh BT. Growth of high density NiSi/SiC core-shell nanowires by hot-wire chemical vapour deposition for electrochemical applications. Materials Characterization. 2017;**132**:187-198

[25] Goh BT, Rahman SA. Study of the growth, and effects of filament to substrate distance on the structural and optical properties of Si/SiC core–shell nanowires synthesized by hot-wire chemical vapor deposition. Materials Chemistry and Physics. 2014;**147**:974-981

[26] Tehrani FS, Goh BT, Muhamad MR, Rahman SA. Pressure dependent structural and optical properties of silicon carbide thin films deposited by hot wire chemical vapor deposition from pure silane and methane gases. Journal of Materials Science: Materials in Electronics. 2013;**24**:1361-1368

[27] Alizadeh M, Ooi PC, bin Omar MF, Dee CF, Goh BT. Solid-state limited nucleation of NiSi/SiC core-shell nanowires by hot-wire chemical vapor deposition. Materials. 2019;**12**:674

[28] Li D, Bulou S, Gautier N, Elisabeth S, Goullet A, Richard-Plouet M, et al. Nanostructure and photocatalytic properties of TiO2 films deposited at low temperature by pulsed PECVD. Applied Surface Science. 2019;**466**:63-69

[29] Goh BT, Wah CK, Aspanut Z, Rahman SA. Structural and optical properties of nc-Si: H thin films deposited by layer-by-layer technique. Journal of Materials Science: Materials in Electronics. 2014;**25**:286-296

[30] Goh BT, Ngoi SK, Yap SL, San Wong C, Dee CF, Rahman SA. Structural and optical properties of the nc-Si: H thin films irradiated by high energetic ion beams. Journal of Non-Crystalline Solids. 2013;**363**:13-19

[31] Rahman MAA, Goh BT, Chiu WS, Haw CY, Mahmood MR, Khiew PS, et al. Aging-and thermal-annealing effects on the vibrational-and microstructural-properties of PECVD grown hydrogenated amorphous silicon carbon nitride thin films. Vibrational Spectroscopy. 2018;**94**:22-30

[32] Hu Z, Li Z, Xia Z, Jiang T, Wang G, Sun J, et al. PECVD-derived graphene nanowall/lithium composite anodes towards highly stable lithium metal batteries. Energy Storage Materials. 2019;**22**:29-39

[33] Al-Masoodi AHH, Nazarudin NFFB, Nakajima H, Tunmee S, Goh BT, Majid WHBA. Controlled growth of silver nanoparticles on indium tin oxide substrates by plasma-assisted hot-filament evaporation: Physical properties, composition, and electronic structure. Thin Solid Films. 2020;**693**:137686

[34] Chang G, Zhang J, Oyama M, Hirao K. Silver-nanoparticle-attached indium tin oxide surfaces fabricated by a seed-mediated growth approach. The Journal of Physical Chemistry B. 2005;**109**:1204-1209

[35] Kuo YL, Juang TY, Chang SH, Tsai CM, Lai YS, Yang LC, et al. Influence of temperature on the formation of silver nanoparticles by using a seed-free photochemical method under sodium-lamp irradiation. ChemPhysChem. 2015;**16**:3254-3263

[36] Dang MC, Dang TMD, Fribourg-Blanc E. Silver nanoparticles ink synthesis for conductive patterns fabrication using inkjet printing technology. Advances in Natural Sciences: Nanoscience and Nanotechnology. 2014;**6**:015003

[37] Xiliang Q, Yang C, Tiesong L, Peng H, Jun W, Ping L, et al. Large-scale synthesis of silver nanoparticles by aqueous reduction for low-temperature sintering bonding. Journal of Nanomaterials. 2014;**2014**:8

[38] Jiang X, Chen W, Chen C, Xiong S, Yu A. Role of temperature in the growth of silver nanoparticles through a synergetic reduction approach. Nanoscale Research Letters. 2011;**6**:32

[39] Zhou D, Bennett SW, Keller AA. Increased mobility of metal oxide nanoparticles due to photo and thermal induced Disagglomeration. PLoS One. 2012;**7**:e37363

[40] Moon J-M, Bae J-H, Jeong J-A, Jeong S-W, Park N-J, Kim H-K, et al. Enhancement of hole injection using ozone treated Ag nanodots dispersed on indium tin oxide anode for organic light emitting diodes. Applied Physics Letters. 2007;**90**:163516

[41] Wei H, Eilers H. From silver nanoparticles to thin films: Evolution of microstructure and electrical conduction on glass substrates. Journal of Physics and Chemistry of Solids. 2009;**70**:459-465

[42] Li W, Seal S, Megan E, Ramsdell J, Scammon K, Lelong G, et al. Physical and optical properties of sol-gel nano-silver doped silica film on glass substrate as a function of heat-treatment temperature. Journal of Applied Physics. 2003;**93**:9553-9561

[43] Kim SH, Choi WI, Kim KH, Yang DJ, Heo S, Yun D-J. Nanoscale chemical and electrical stabilities of graphene-covered silver nanowire networks for transparent conducting

electrodes. Scientific Reports. 2016;**6**:33074

[44] Milczarek G, Rebis T, Fabianska J. One-step synthesis of lignosulfonate-stabilized silver nanoparticles. Colloids and Surfaces B: Biointerfaces. 2013;**105**:335-341

[45] Hoflund GB, Hazos ZF, Salaita GN. Surface characterization study of Ag, AgO, and Ag_2O using x-ray photoelectron spectroscopy and electron energy-loss spectroscopy. Physical Review B. 2000;**62**:11126

[46] Agnihotri S, Mukherji S, Mukherji S. Size-controlled silver nanoparticles synthesized over the range 5-100 nm using the same protocol and their antibacterial efficacy. RSC Advances. 2014;**4**:3974-3983

[47] Schinca D, Scaffardi L. Core and shell sizing of small silver-coated nanospheres by optical extinction spectroscopy. Nanotechnology. 2008;**19**:495712

[48] Yun S, Hong S, Acapulco JA, Jang HY, Ham S, Lee K, et al. Close-packed two-dimensional silver nanoparticle arrays: Quadrupolar and dipolar surface plasmon resonance coupling. Chemistry-A European Journal. 2015;**21**:6165-6172

[49] Kinnan MK, Chumanov G. Plasmon coupling in two-dimensional arrays of silver nanoparticles: II. Effect of the particle size and interparticle distance. The Journal of Physical Chemistry C. 2010;**114**:7496-7501

[50] Kumar GA, Reddy MR, Reddy KN. Structural and optical properties of AgO thin films grown by RF reactive magnetron sputtering technique, advanced nanomaterials and emerging engineering technologies (ICANMEET). In: 2013 International Conference on, IEEE. 2013. pp. 354-356

[51] Ida Y, Watase S, Shinagawa T, Watanabe M, Chigane M, Inaba M, et al. Direct electrodeposition of 1.46 eV bandgap silver (I) oxide semiconductor films by electrogenerated acid. Chemistry of Materials. 2008;**20**:1254-1256

[52] Chen S-H, Li Y-R, Yu C-F, Lin C-F, Kao P-C. Enhanced luminescence efficiency of Ag nanoparticles dispersed on indium tin oxide for polymer light-emitting diodes. Optics Express. 2013;**21**:26236-26243

[53] Akbi M. Effect of arcing in air on the photoelectric work function of silver-based contacts. IEEE Transactions on Plasma Science. 2015;**43**:637-642

[54] Kim C, Kim YH, Noh YY, Hong SJ, Lee MJ. Improved charge injection of metal oxide thin-film transistors by stacked electrodes of indium tin oxide nanoparticles and silver nanowires. Advanced Electronic Materials. 2018;**4**:1700440

[55] Klein A, Körber C, Wachau A, Säuberlich F, Gassenbauer Y, Harvey SP, et al. Transparent conducting oxides for photovoltaics: Manipulation of fermi level, work function and energy band alignment. Materials. 2010;**3**:4892-4914

[56] Bühler G, Thölmann D, Feldmann C. One-pot synthesis of highly conductive indium tin oxide nanocrystals. Advanced Materials. 2007;**19**:2224-2227

[57] Nwanya AC, Ugwuoke PE, Ezekoye BA, Osuji RU, Ezema FI. Structural and optical properties of chemical bath deposited silver oxide thin films: Role of deposition time. Advances in Materials Science and Engineering. 2013;**2013**:8

[58] Varkey A, Fort A. Some optical properties of silver peroxide (AgO) and silver oxide (Ag2O) films produced

by chemical-bath deposition. Solar Energy Materials and Solar Cells. 1993;**29**:253-259

[59] Jeong J-A, Lee J, Kim H, Kim H-K, Na S-I. Ink-jet printed transparent electrode using nano-size indium tin oxide particles for organic photovoltaics. Solar Energy Materials and Solar Cells. 2010;**94**:1840-1844

[60] Chong SK, Goh BT, Aspanut Z, Muhamad MR, Dee CF, Rahman SA. Synthesis of indium-catalyzed Si nanowires by hot-wire chemical vapor deposition. Materials Letters. 2011;**65**:2452-2454

[61] Chong SK, Goh BT, Aspanut Z, Muhamad MR, Dee CF, Rahman SA. Radial growth of slanting-columnar nanocrystalline Si on Si nanowires. Chemical Physics Letters. 2011;**515**:68-71

[62] Maruyama T, Arai S. Electrochromic properties of cobalt oxide thin films prepared by chemical vapor deposition. Journal of the Electrochemical Society. 1996;**143**:1383-1386

IntechOpen

IntechOpen